THE JOURNAL OF COMPARATIVE NEUROLOGY 429:372–387 (2001)

Size Gradients of Barreloids in the Rat Thalamus

SEBASTIAN HAIDARLIU* AND EHUD AHISSAR
Department of Neurobiology, The Weizmann Institute of Science, Rehovot 76100, Israel

ABSTRACT

The spatial organization of the anatomical structures along the trigeminal afferent pathway of the rat conserves the topographical order of the receptor sheath: The brainstem barrelettes, thalamic barreloids, and cortical barrels all reflect the arrangement of whiskers across the mystacial pad. Although both the amount of innervation in the mystacial pad and the size of cortical barrels were shown previously to exhibit increasing gradients toward the ventral and caudal whiskers, whether similar gradients existed in the brainstem and thalamus was not known. Here, the authors investigated the size gradients of the barreloids in the ventral posteromedial nucleus of the rat thalamus. Because the angles used to cut the brain were crucial to this study, the optimal cutting angles were determined first for visualization of individual barreloids and of the entire barreloid field. Individual barreloids, arcs, and rows as well as entire barreloid fields were clearly visualized using cytochrome oxidase staining of brain slices that were cut with the optimal cutting angles. For the first five arcs (including straddlers), the length of barreloids increased in the direction of dorsal-to-ventral whiskers and of caudal-to-rostral whiskers. These gradients reveal an inverse relationship between the size of barreloids and whiskers (length and follicle diameter) along arcs and rows. The largest barreloids in the ventral posteromedial nucleus were those that represent whiskers C2–C4, D2–D4, and E2–E4, which are neither the largest nor the most innervated whiskers in the mystacial pad. This implies that the extended representation is not merely a reflection of peripheral innervation biases and probably serves an as yet unknown processing function. J. Comp. Neurol. 429:372–387, 2001. © 2001 Wiley-Liss, Inc.

Indexing terms: ventral posteromedial thalamic nucleus; vibrissal representation

The ascending trigeminal system of rodents contains clear structural representations of the whisker pad in the brainstem (*barrelettes*; Ma, 1991), thalamus (*barreloids*; Van der Loos, 1976), and cortex (*barrels*; Woolsey and Van der Loos, 1970). Barreloids and barrels (in the thalamus and cortex, respectively) are the anatomical structures that contain most of the neurons of the lemniscal thalamocortical loops (Chmielowska et al., 1989; Lu and Lin, 1993). The spatial organization of these representations probably facilitates the processing of spatially encoded vibrissal information, a processing that fits the functional properties of lemniscal neurons (Ahissar and Zackenhouse, 2000; Ahissar et al., 2000). Indications of the computational significance of the spatial parameters of these anatomical structures (vibrissal representations) can be obtained by comparing them with spatial parameters across the mystacial pad. So far, such comparisons had been done only for the cortical vibrissal structures—the barrels (Lee and Woolsey, 1975; Welker and Van der Loos, 1986; Rice, 1995). Information about the three-dimensional structure of the ventral posteromedial nucleus (VPM), the size of the barreloids, and their organization along arcs and rows is scarce. One major obstacle for obtaining detailed descriptions of the spatial organization in the VPM is that the long axes of barreloids do not coorient with the traditional stereotaxic planes (coronal, parasagittal, and horizontal) that are used to reveal brain morphology (Van der Loos, 1976; Land and Simons, 1985; Sugitani et al., 1990).

Barreloids were first described in the brains of mice (Van der Loos, 1976). In young mice, the barreloid map is apparent in horizontal brain slices stained for cytochrome oxidase (CO; Yamakado, 1999). However, in adult mice, visualization of barreloids requires oblique cutting angles

Grant sponsor: The Minerva Foundation (Germany); Grant sponsor: Center for Absorption of Scientists, Ministry of Absorption, Israel.

*Correspondence to: Sebastian Haidarliu, Department of Neurobiology, The Weizmann Institute of Science, Rehovot 76100, Israel.
E-mail: sebastian.haidarliu@weizmann.ac.il

Received 12 July 2000; Revised 22 September 2000; Accepted 10 October 2000

© 2001 WILEY-LISS, INC.

(Van der Loos, 1976; Woolsey et al., 1979). With young rats, standard cutting angles also allow partial visualization of the barreloid fields (Belford and Killackey, 1979; Ivy and Killackey, 1982). However, by 15 days after birth, these barreloid patterns are no longer clear with standard cutting planes (Ivy and Killackey, 1982). To visualize barreloids in slices of adult rat brains, the sectioning orientations should be different than those of the traditional planes. Based on electrophysiological recordings, Sugitani et al. (1990) presented a detailed map of the VPM barreloids of the adult rat indicating that the optimal plane for visualizing the barreloid map should be approximately 30° to the horizontal plane. Using sections cut at 45° to the horizontal plane, Land and colleagues were able to visualize barreloid fields in adult rats (Land and Simons, 1985; Land et al., 1995). Using an oblique sagittal plane, the rod-like structure of single barreloids was revealed (Land et al., 1995). The three-dimensional anatomical organization of the barreloids thus obtained confirmed the organization predicted from electrophysiological studies (Waite, 1973; Sugitani et al., 1990). However, the dimensions of individual barreloids were not revealed.

To reveal the dimensions of individual barreloids and possible size gradients, determination of the orientation of the long axes of barreloids as well as of the organization of barreloids along individual rows and arcs was required. Because barreloids are best visualized in neonatal rat tissue stained for mitochondrial markers (Price, 1995), we first used young rats (5–14 days after birth) for histological preparations and later compared the data obtained from young rats with those from adult rats. Using a histochemical reaction for CO activity and radial cuttings, we determined the optimal planes for clear visualization of the entire barreloid field, representations of the entire set of individual arcs, and representations of the entire set of individual rows of barreloids. In brain slices that were obtained using these optimal sectioning planes, sizes of individual barreloids could be measured accurately, and, thus, size gradients could be determined for individual rows and arcs.

MATERIALS AND METHODS

Animals

Both young (n = 62 animals) and adult (n = 38 animals) albino Wistar rats (obtained from The Animal Breeding Unit of The Weizmann Institute of Science) were used. Pups from 12 litters (each containing 4–12 rats of both sexes) were used as subjects 5 days, 6 days, 7 days, 9 days, 13 days, and 14 days after birth (2 litters were used for each age group). Brains were obtained from 35 adult male rats (weight, 250–350 g) that were used for electrophysiological studies in which recordings were made from various stations of the ascending trigeminal pathways, including the VPM (Haidarliu et al., 1999; Ahissar et al., 2000). Three adult rats that were not exposed to electrophysiological studies were also used. Young and adult animals were killed with Pental (0.1 ml and 0.5 ml pro capito, respectively, i.p.); perfused transcardially with 2.5% glutaraldehyde, 0.5% paraformaldehyde, and 5% sucrose in 0.1 M phosphate buffer, pH 7.4; and then decapitated. The brains were removed and stored in postfixation solution until sectioned, usually not more than 24 hours later. The procedures for animal maintenance, manipulations, and surgeries were approved by the Institute's Animal Care and Use Committee and conformed to National Institutes of Health guidelines.

Preparation and staining of brain slices

Detailed examination of the barreloid architecture in the VPM usually was achieved by preparing slices of brain tissue and staining them histochemically for CO to detect endogenous oxidative activity of neurons and dendrites (Wong-Riley, 1989). To determine the optimal angles of the planes for visualizing barreloid architecture, we first cut the right brain hemispheres of three young rats and three adult rats horizontally at the upper or lower pole of the VPM. Using the line where the horizontal plane crosses the sagittal plane as an axis, each consecutive slice was cut at an increasing angle with respect to the horizontal plane. Among the consecutive slices obtained in this manner, some were cut perpendicular to the long axes of the barreloids (which provided the best visualization of the entire barreloid field), and some were cut parallel to the long barreloid axes (in which arcs were best visualized). With the left hemispheres, a similar radial slicing was performed; however, the cutting planes used were vertical, with the center of rotation of the cutting plane close to the sagittal plane and 3.0–4.5 mm caudal to Bregma. The latter permitted determination of the cutting angle required for visualization of barreloid rows. Sections were processed histochemically for CO as previously described (Haidarliu and Ahissar, 1997), except that the incubation with diaminobenzidine was performed at room temperature or at 4°C, and not at 37°C. For all sequential slices depicted in the figures, the order of cutting was from a to e, from a to f, from a to g, or from a to h.

Preparation of figures and photomontages

All figures were prepared from digital images. An Axiolab microscope (Zeiss, Oberkotchen, Germany) equipped with low-magnification objectives (×2.5 and ×1.25) was used to obtain brightfield images of CO- and Nissl-stained brain slices. For image capture, Adobe Premiere 5.0 software (Adobe Systems; Mountain View, CA) and a ColorSync Display screen (20 inch) were used. All of the digital images obtained were imported into Adobe Photoshop software (version 4.0; Adobe Systems). Separate images were photomontaged into a composite assembly. Only minimal adjustments in contrast and brightness were made during editing of the images depicted in Figures 1–6. Structural details were distinct both in color prints and in black-and-white prints of the images. Distortion and perspective transformation features of Photoshop were used to produce the photomicrographs shown in Figure 12a,b,d.

Morphometric analysis

Images of thalamic slices that were cut consecutively in various planes of the VPM were grouped such that all of the barreloid arcs and/or barreloid rows of the dorsolateral barreloid subfield (DLBSF) were present in a single montage. A transparent sheet was attached to each such montage, and the barreloid contours were traced manually. The dimensions of barreloid parameters [the length of long axes and the two diameters (d, small diameter; D, large diameter) of transverse sections] were measured manually from the arc and field planes, respectively; average dimensions and standard errors of the mean for the

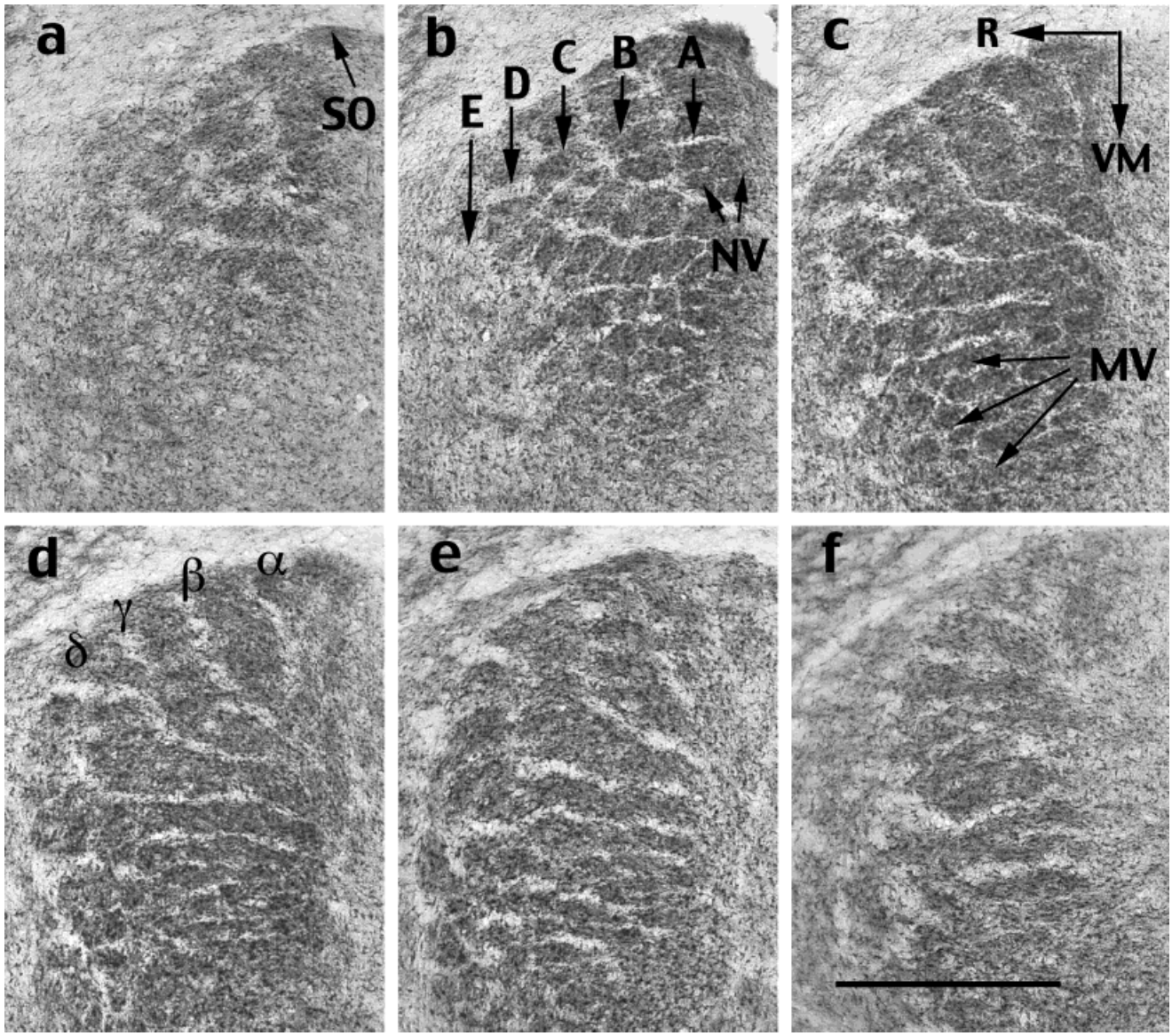

Fig. 1. Histochemical staining for cytochrome oxidase (CO) of oblique, consecutive slices (50° and 30° clockwise to the sagittal plane when viewed caudally and dorsally, respectively) through the right hemisphere of a 7-day-old rat. **a–f:** Photomicrographs showing consecutive sections from dorsomedial to ventrolateral. A–E, barreloid rows; MV, barreloids representing microvibrasse; NV, barreloids representing nasal vibrasse; SO, barreloids representing supraorbital vibrissae; R, rostral; VM, ventromedial; α, β, γ, and δ, barreloids representing straddlers. Scale bar = 0.5 mm.

barreloids that were measured in this manner were calculated. For young rats and adult rats, the lengths of whiskers and the diameters of follicles in the mystacial pad were measured, and the results were compared with the lengths of the corresponding barreloids. Except for two young rats, the measurements of barreloids and whiskers were performed in different animals. The diameters of the vibrissal follicles were measured directly from the calibrated images of slices that were cut parallel to the skin through the mystacial pad of seven young rats (7 days old) and eight adult rats and that were stained with cresyl violet, as previously described (Haidarliu and Ahissar, 1997), to clearly visualize the follicles.

RESULTS

Orientation of the barreloid field

To determine the orientation of barreloids, sectioning was performed in radial directions that had a fixed, common line that projected to the most dorsal and most ventral poles of the VPM in the sagittal plane in the brains of three adult rats and three young rats. All of the slices were cut such that their thickness was 60–70 μm at the central part of the VPM. Examination of all sections from these six rats revealed that the barreloid field is shaped like a rotational ellipsoid obtained by rotation around its short axis and flattened in the dorsomedial to ventrolateral

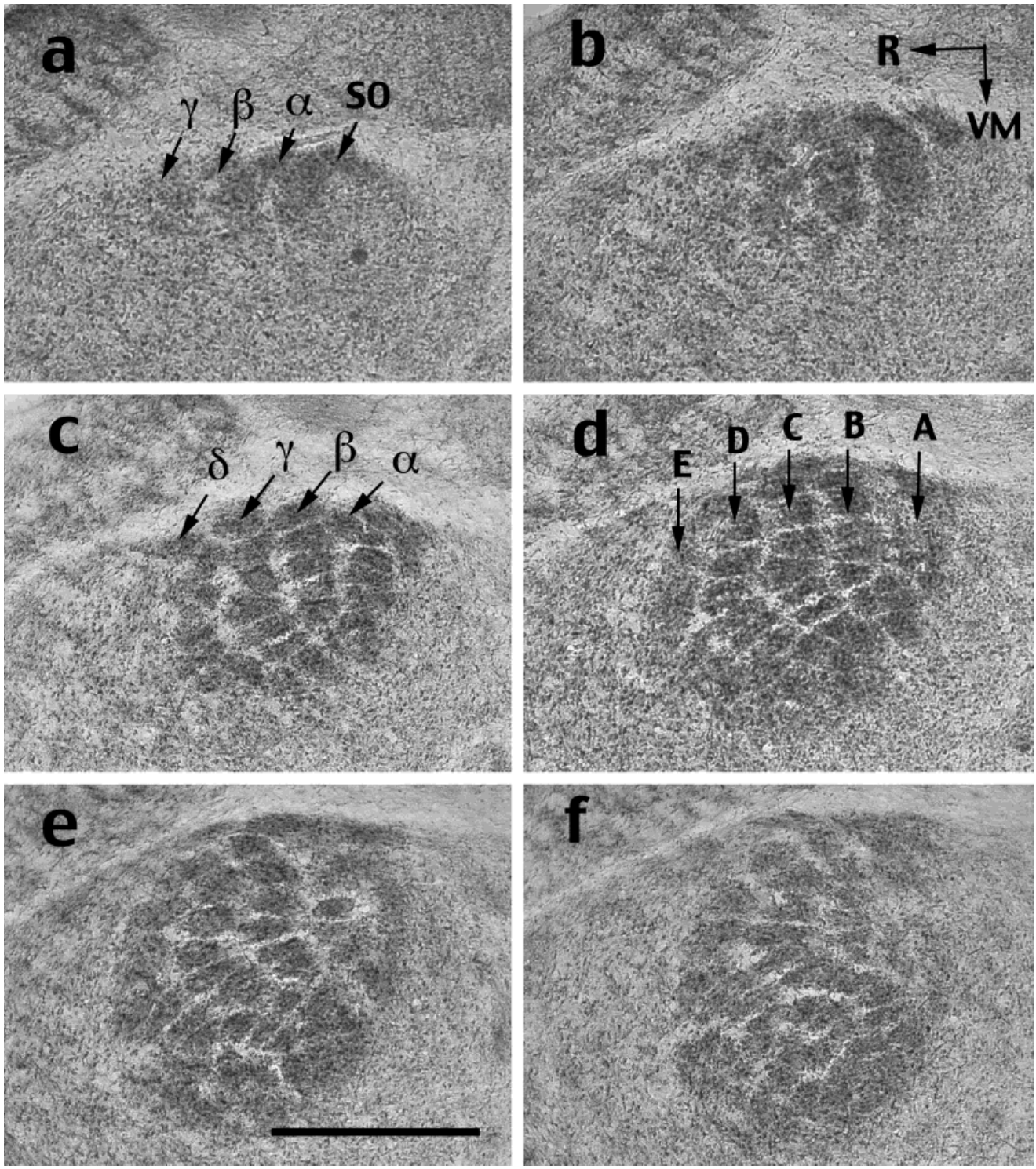

Fig. 2. **a–f:** Histochemical staining for CO of oblique, consecutive slices (30° clockwise to the sagittal plane when viewed either caudally or dorsally) through the right hemisphere of a 9-day-old rat. For abbreviations and sectioning order, see Figure 1. Scale bar = 0.5 mm.

directions. Thus, the three-dimensional structure of the VPM resembles a disc in which the long axes of individual barreloids are perpendicular to the flattened surface and represent the shortest axis of the VPM. The longest axis of such an "ellipsoid" was situated from ventromedial to dorsolateral at an angle of 50° clockwise to the sagittal

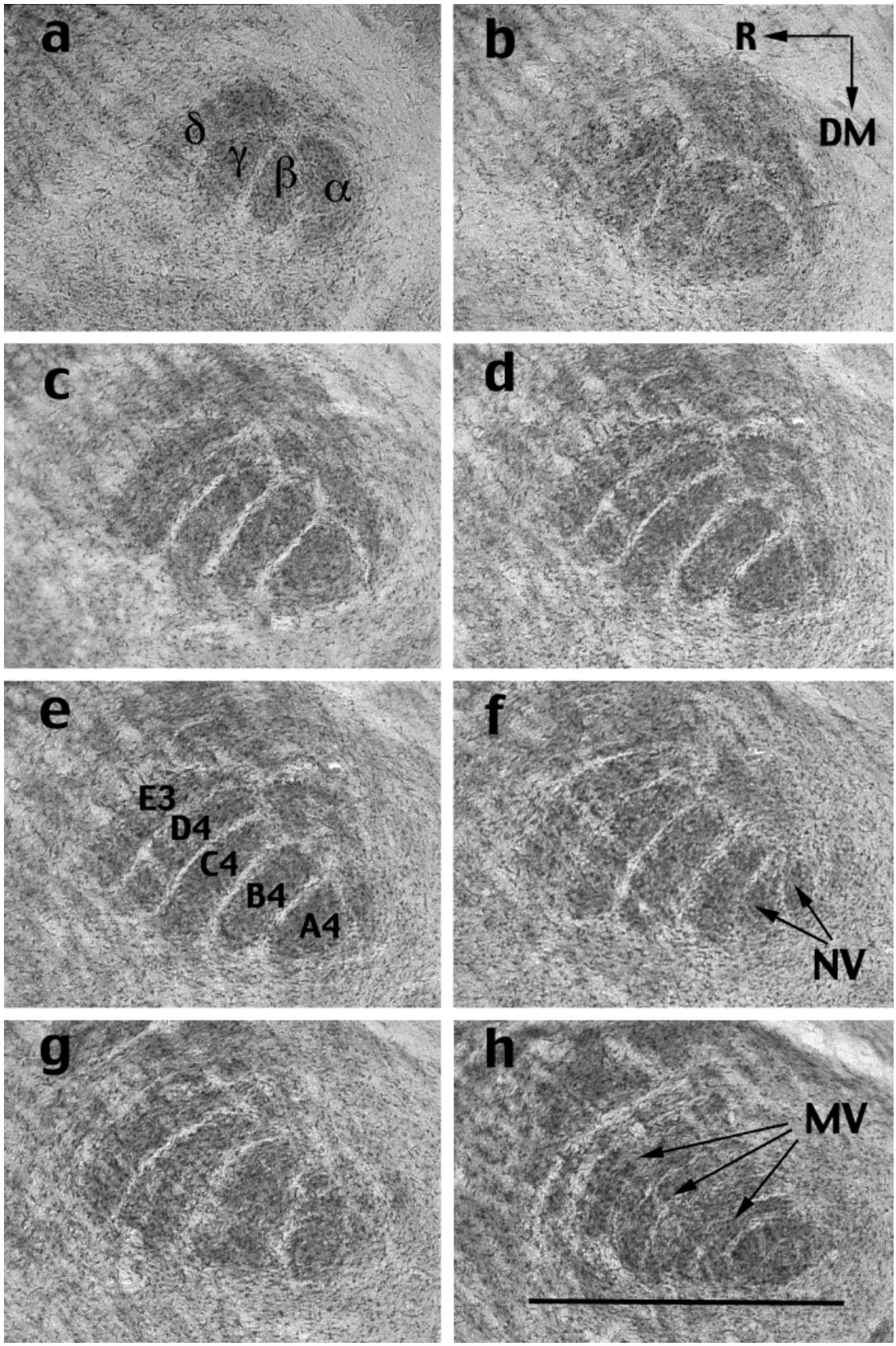

Fig. 3. Visualization of individual arcs by histochemical staining for CO of oblique, consecutive slices through the right hemisphere of a 7-day-old rat. The plane of section was 40° counterclockwise to the sagittal plane (when viewed caudally). Slices were 70 μm thick. **a–h:** Consecutive sections from dorsolateral to ventromedial containing barreloids that represent four straddlers and the arcs of barreloids. DM, dorsomedial. For abbreviations, see Figure 1. Scale bar = 1 mm.

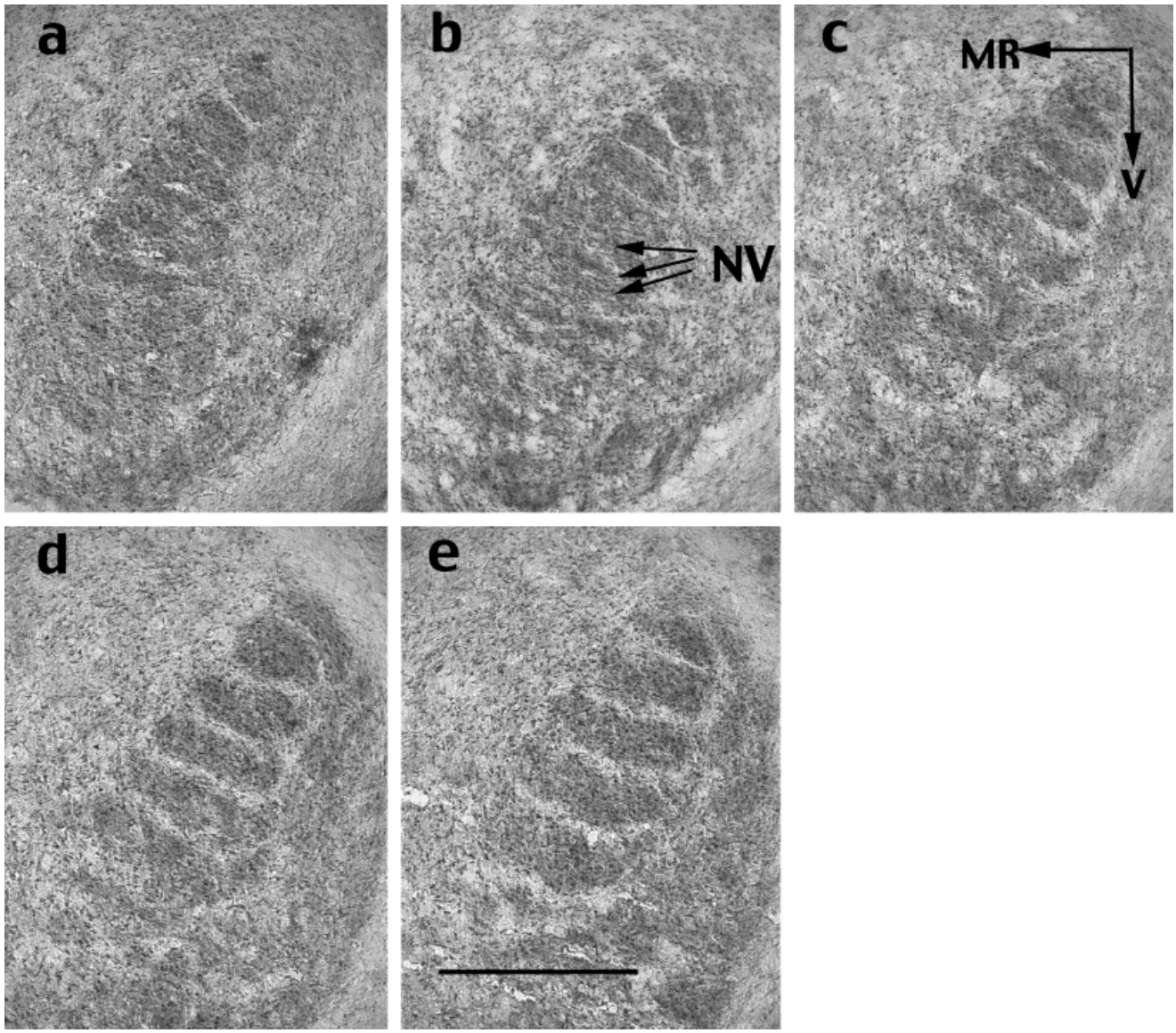

Fig. 4. Visualization of individual barreloid rows by histochemical staining for CO of consecutive slices (from caudomedial to rostrolateral; 70 μm thick; every other section is shown). The brain of a 5-day-old rat was sliced vertically; the angle of section was 30° clockwise to the coronal plane when viewed dorsally. **a–e:** Slices representing rows A–E, respectively, of the barreloid field of the right hemisphere (caudal view). MR, mediorostral; NV, barreloids representing nasal vibrissae; V, ventral. Scale bar = 0.5 mm.

plane (when viewed caudally from the right hemisphere), and the median axis was in the mediocaudal-to rostrolateral-direction at an angle of 30° clockwise to the sagittal plane (when viewed dorsally). When the VPM was cut in the plane that contained the longest and median barreloid axes, almost all of the barreloids could be seen in a single slice (Fig. 1), because they were cut essentially perpendicular to their longest axes. Images of six consecutive slices of the VPM, from mediodorsal (Fig. 1a) to ventrolateral (Fig. 1f), are depicted in Figure 1. In the upper caudolateral area of the barreloid field, barreloids that correspond to the supraorbital (SO) vibrissae were usually seen (one SO barreloid is present in Fig. 1a). Rostral to the SO barreloid in Figure 1a, an arc of strad-

Fig. 5 (Overleaf). Structure of the adult ventral posteromedial nucleus (VPM) shown in histochemical staining for CO of slices of adult rat brains. **a:** Oblique slice of the right hemisphere cut at angles of 50° and 30° clockwise to the sagittal plane when viewed caudally and dorsally, respectively, to visualize the entire barreloid field. **b:** Mediolateral view of the right VPM cut oblique at an angle of 40° counterclockwise to the sagittal plane (when viewed caudally) to visualize barreloid arcs. **c:** Rostral view of the right hemisphere cut vertically at an angle of 30° clockwise to the coronal plane (when viewed dorsally) to visualize barreloid rows. Camera lucida drawings (**d–f**) and schematic drawings demonstrating the cutting planes (**g–i**) are shown for the slices depicted in a–c, respectively. D, dorsal; DM, dorsomedial; L, lateral; LC, laterocaudal; R, rostral; V, ventral; and VM, ventromedial. Scale bars = 1 mm.

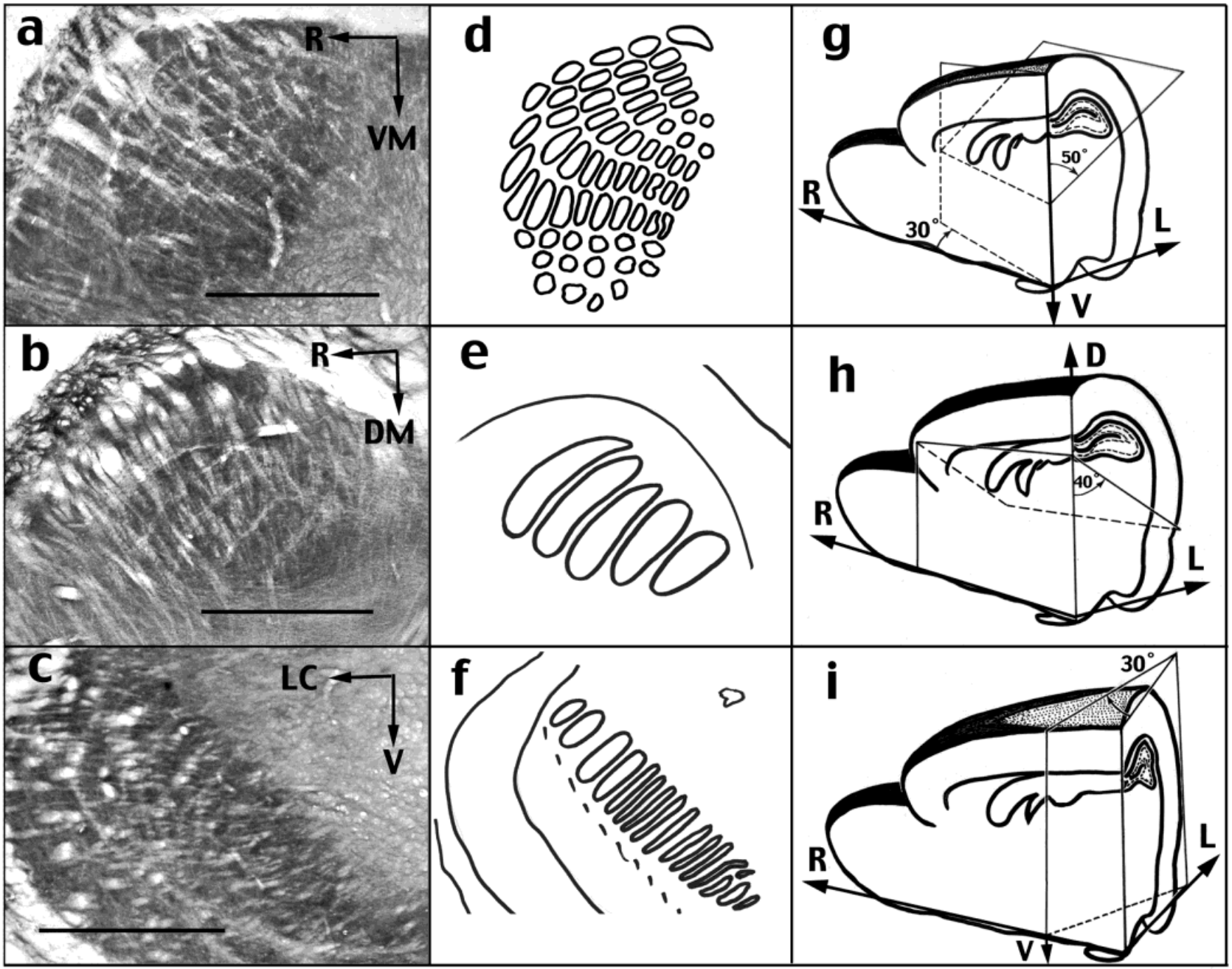

Figure 5 (Overleaf)

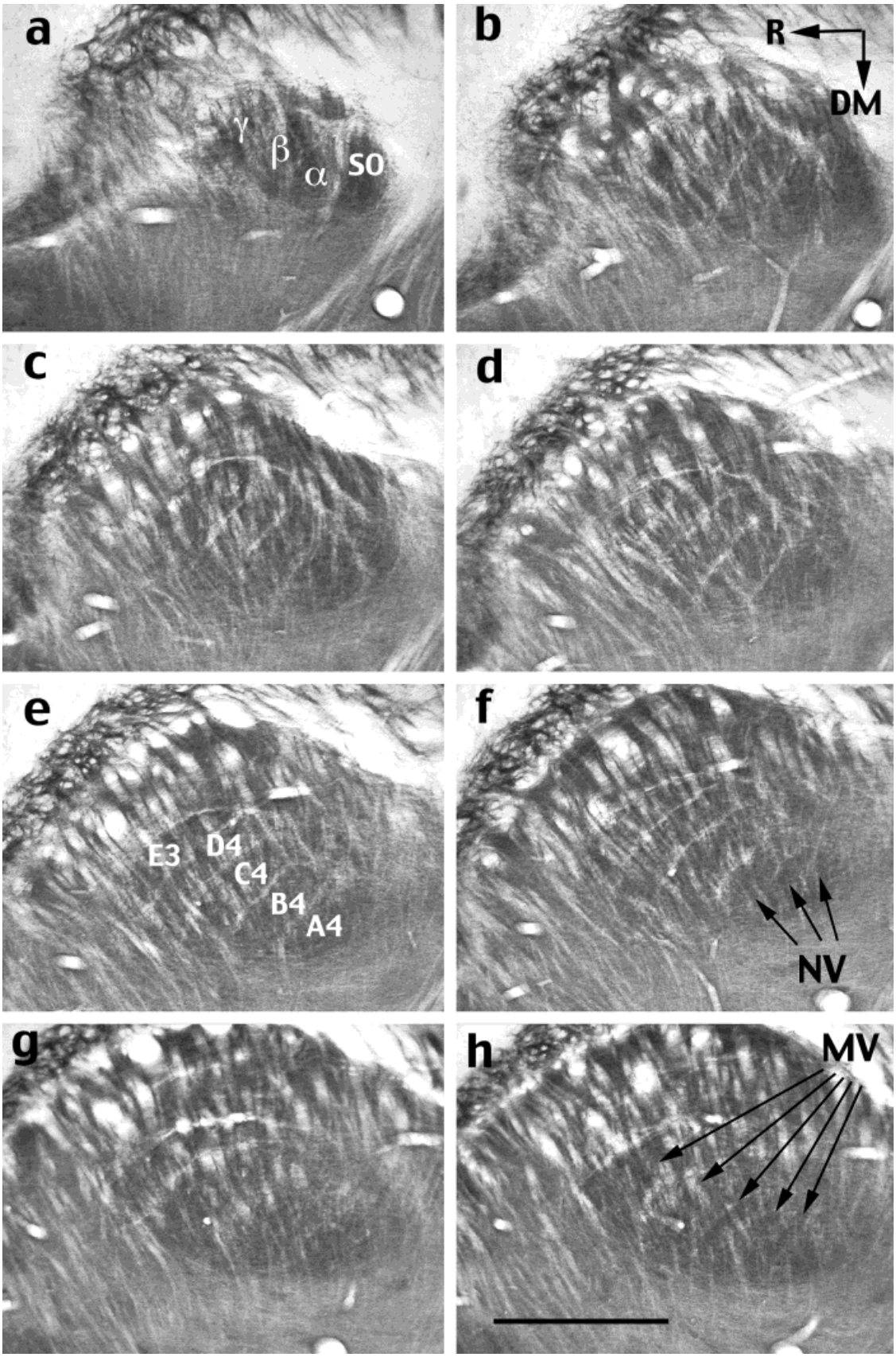

Fig. 6. **a–h:** Histochemical staining for CO of consecutive, oblique slices (cut 40° counterclockwise to the sagittal plane when viewed caudally) of the right hemisphere of an adult rat. For abbreviations and sectioning order, see Figure 3. Scale bar = 1 mm.

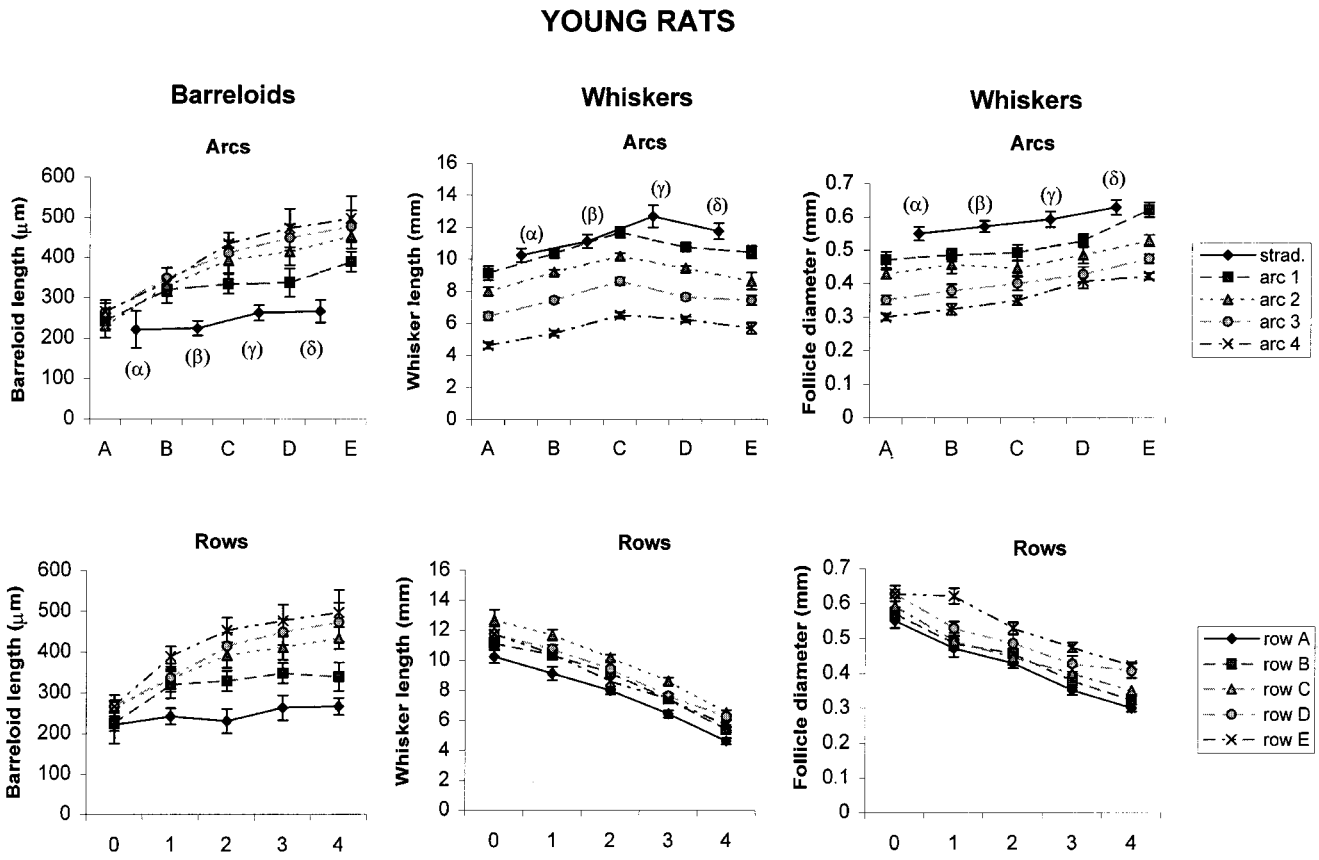

Fig. 7. Gradients of barreloid lengths (n = 5 rats), whisker lengths (n = 8), and vibrissal follicle diameters (n = 7) along the arcs and rows of young rats. The mean ± S.E.M. values are depicted. The straddler δ was considered as whisker "0" in both row D and row E.

dler barreloids [α, β, γ, and δ in Fig. 1d; in the ventromedial direction, row A of barreloids (corresponding to vibrissae A1–A4) can be seen in Fig. 1b]. During serial slicing, barreloids of row A were the first to disappear (see Fig. 1d), because they are the shortest. In the ventromedial continuation of rows A and B, usually five or six thin barreloids were seen (Fig. 1c) that corresponded to the nasal vibrissae (NV). The spaces between neighboring rows of barreloids were larger than the spaces between barreloids within the same row. Rows C–E turned in a caudal direction with a slightly blunt angle, starting at the 4th or 5th barreloid in the row. Ventromedial to the DLBSF, which represents mystacial vibrissae, thin barreloids were observed that correspond to microvibrissae according to the terminology of Brecht et al. (1997).

When the plane of cutting was parallel to the longest axis of the entire VPM (as in Fig. 1), the septa between the rows of barreloids in the DLBSF were seen distinctly. However, this sectioning plane did not appear to be perpendicular to the longest axis of individual barreloids in the DLBSF. Because the thickness of the slices (60 μm) was of the same order of magnitude as the length of the shortest axis of the barreloids, along the rows, the septa between the barreloids were barely seen. The visibility of the septa in rows improved as the angle between the horizontal and cutting planes decreased (see Fig. 2). Individual barreloids were seen distinctly in such slices, because both the septa that separate neighboring rows and those that separate barreloids within the rows became visible to a similar extent. In the first consecutive slices of the DLBSF shown in Figure 2a–d, large barreloids that represent vibrissae of the mystacial pad were the first to become visible, followed by a field with thin barreloids, which represent microvibrissae (Fig. 2f).

Arrangement of the barreloids in arcs

The arrangement of the barreloids in arcs was determined by examining brain slices that were obtained by radial cuttings in which the line of intersection of cutting planes was horizontal in the sagittal plane, and the angle for each consecutive slice was increased by 2–3°. The resulting serial slices from young and adult rats were thickest at the lateral border, about 60–70 μm in the middle of the slice, and thinnest at the medial edge. When the cutting plane was parallel to the long axes of the barreloids, slices formed angles of about 50° clockwise to the horizontal plane, when viewed caudally from the right hemisphere. In these slices, the long axes of the barreloids also formed an angle of 30° clockwise to the coronal plane when viewed dorsally (for orientations, see Fig. 5).

To visualize arcs, consecutive slices (Fig. 3) were obtained by cutting at an angle of 40° counterclockwise to the horizontal plane, which was almost perpendicular to the angle used to cut the slices depicted in Figure 1. In the

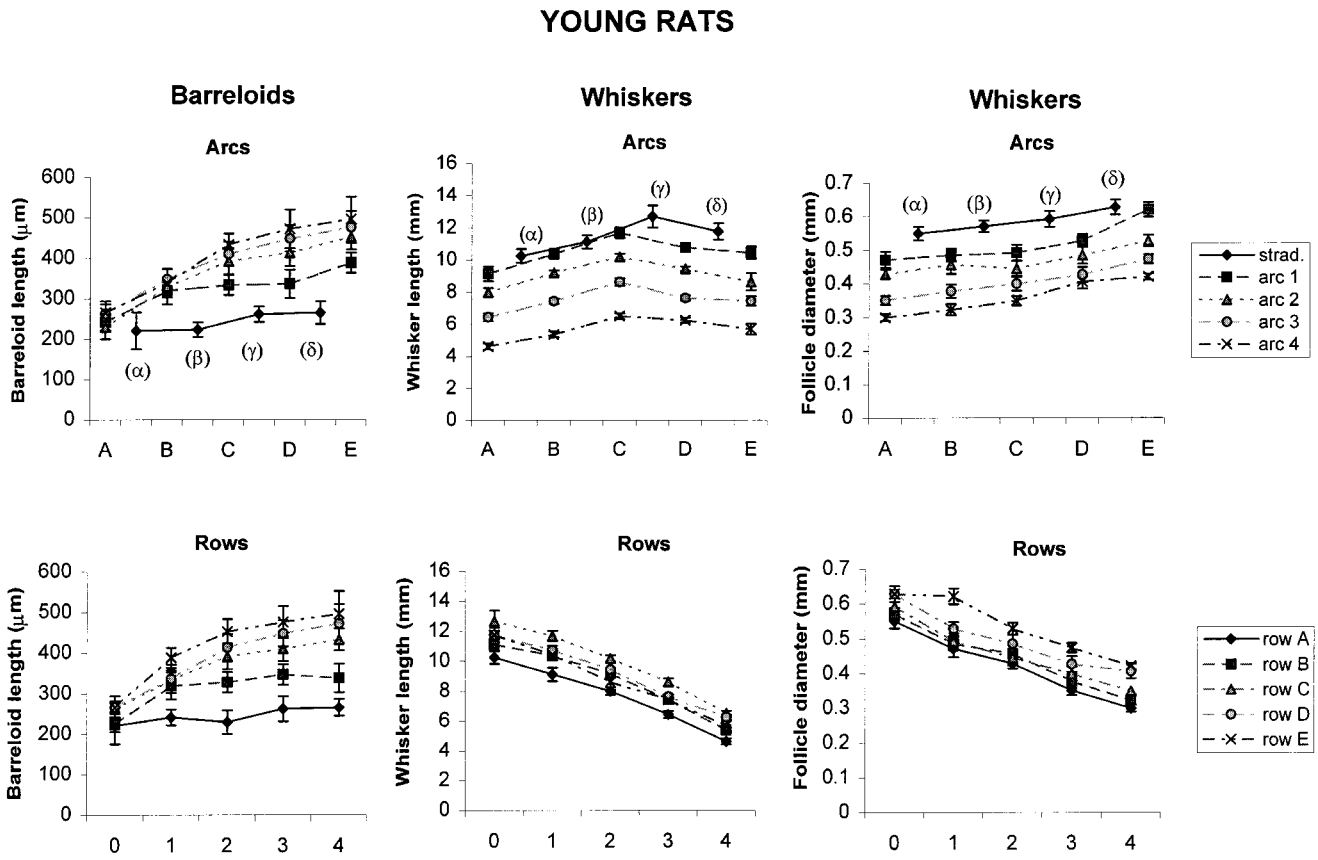

Fig. 8. Gradients of barreloid lengths (n = 7 rats), whisker lengths (n = 7), and vibrissal follicle diameters (n = 7) along the arcs and rows of adult rats (for details, see Fig. 7, legend).

slices depicted in Figure 3, all of the straddlers and all of the barreloids that formed consecutive arcs were cut parallel to their long axes. Thin and long barreloids that correspond to microvibrissae were seen in the slices that contained the most ventromedial part of the VPM (Fig. 3h).

The curvatures of the long axes of the barreloids (see Fig. 3d–f) were directed rostrally and were most pronounced for barreloids of rows C–E; and were absent or were less pronounced for the straddlers and the shortest barreloids (A1, B1, A2, B2, and A3). Along the arcs, a gradient of barreloid length was observed in which row A had the shortest barreloids, and row E had the longest barreloids.

Structure of barreloids in individual rows

To visualize individual rows, consecutive slices were obtained using an oblique, vertical cutting plane from caudolateral to rostromedial at an angle of 30° clockwise to the coronal plane when viewed dorsally (for right hemispheres). In slices that were obtained in this manner, rows of barreloids were distinctly seen (Fig. 4). The barreloid rows resembled truncated pyramids that were comprised of almost regularly arranged barreloids, reminiscent of side-by-side cylinders. In these pyramid-like structures, the shortest barreloids, which represented caudal whiskers, were at the top, and the longest barreloids were at the base (Fig. 4a–e). In each consecutive slice, the length of the barreloids was noticeably longer, corresponding to the increasing length seen in each of the arcs (see Fig. 3). In slices that were obtained with optimal parameters for viewing barreloid rows, all of the barreloids (except those in row E) appeared to be cylindrical and straight, not bent as seen in the arc views. In the barreloids of row E, a slight curvature was observed (Fig. 4e). The barreloids of the most caudal rows in the VPM, rows A and B, are depicted in Figure 4a,b, respectively. In the ventromedial continuation of rows A and B, a few thin barreloids, corresponding to the NV (Fig. 1b,c), also were seen clearly. Rows C (Fig. 4c) and D (Fig. 4d) had four and five large barreloids, respectively, that were separated from each other by septa with a constant width of ≈15 μm. Ventromedial to row C, two large barreloids were seen that were separated from each other by larger septa of ≈30 μm and belonged to rows D and E. The width of the septa between barreloids in the same row seems to be half of the width of the septa between barreloids of neighboring rows. In all rows, a gradient of barreloid length was observed, with longer barreloids representing more rostral whiskers.

Barreloids in the brain of the adult rat

When we used traditional methods for cutting the brains of adult rats in the coronal, sagittal, or horizontal planes, barreloids were usually seen but were not identi-

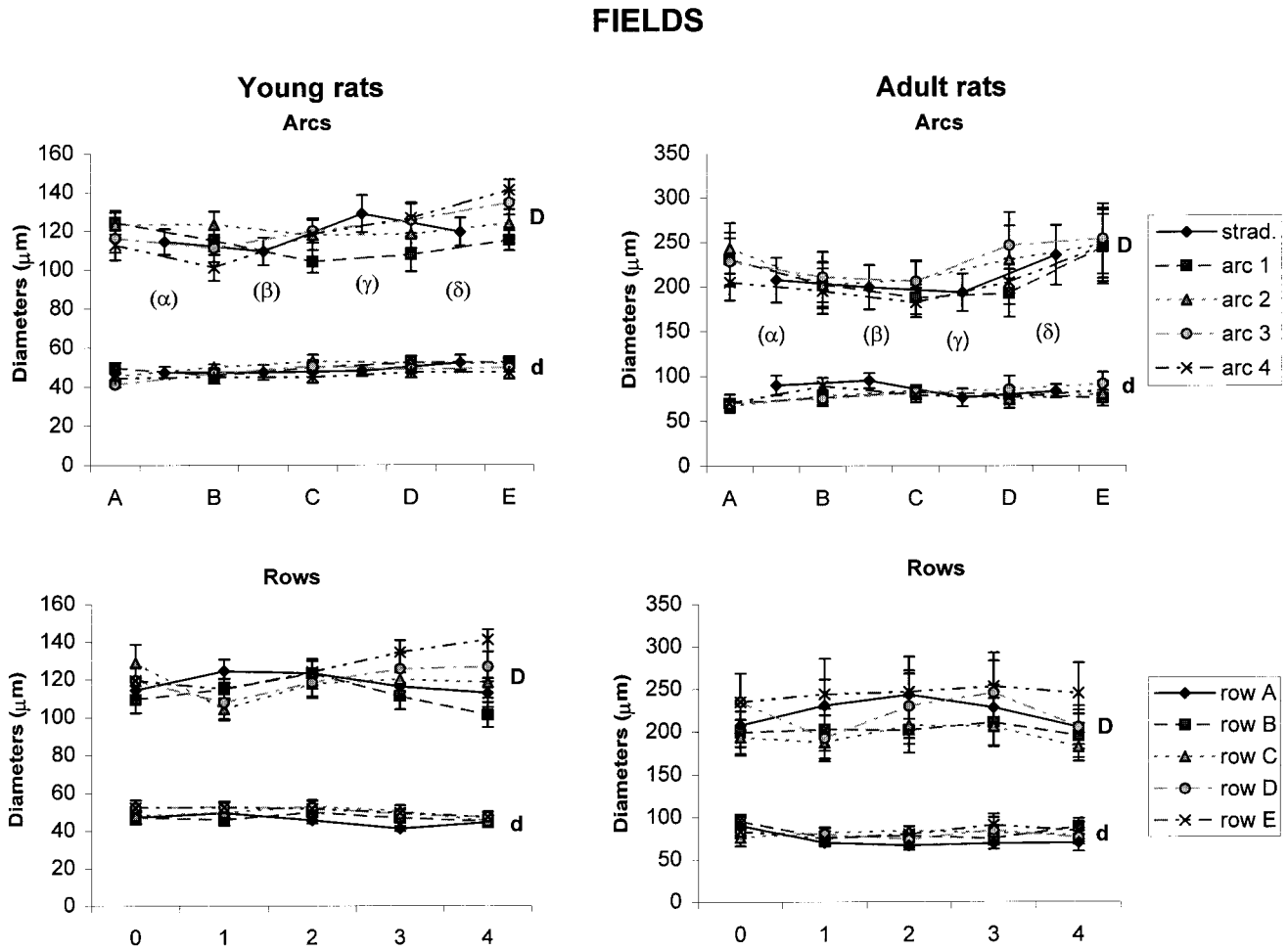

Fig. 9. Gradients of the ellipsoidal diameters (d, small diameter; D, large diameter) of the barreloids along the arcs and rows of young (n = 9) and adult (n = 6) rats.

fiable. However, when we used angles that are optimal for visualization of barreloids in young rats (Fig. 5g–i), visualization of barreloids in adult rats improved significantly. Slices of right brain hemispheres from adult rats (Fig. 5a) were obtained by cutting 50° clockwise to the sagittal plane, when viewed caudally, and 30° to the same plane, when viewed dorsally (see schematic drawing in Fig. 5g). The appearance of the VPM in adult rats differed from that in the young rats, because all of the barreloids in the adult rats had been penetrated by bundles of myelinated nerve fibers that crossed the VPM, primarily in the medial-to-lateral direction. The length of the entire VPM in the rostrocaudal direction was ≈600 μm in young rats (Fig. 1d) and ≈1 mm in adult rats (Fig. 5a,b). In adult rats, the shapes of transversal sections of individual barreloids were oval (Fig. 5d), as in the pups (Figs. 1, 2). When brain hemispheres of adult rats were cut at angles conducive to visualizing barreloid arcs (Fig. 5b) and barreloid rows (Fig. 5c), the barreloids were about two times longer than in young animals (Fig. 5e,f), but their boundaries were less distinct.

Despite the less distinct barreloid boundaries observed in brains from adult rats, consecutive sections made in the planes of the long axes of the barreloids yielded images similar to those obtained from brains of young rats (compare Fig. 3 with Fig. 6). Consecutive slices that represent individual vibrissal arcs in adult rats are depicted in Figure 6. The spatial organization of the straddlers (Fig. 6a), arcs 1–5 (Fig. 6b–f), and the microvibrissae (Fig. 6h) in adult rats resembled those observed in young rats (Fig. 3).

Dimensions of barreloids and whiskers

The dimensions of all the barreloids of the first five arcs (including straddlers) of young and adult rats were measured from the calibrated photomontages and were compared with whisker lengths and follicle sizes. Three barreloid dimensions were measured: the length along the long axis (as observed in the views of the arcs and rows shown in Figs. 3–6) and the two diameters (d and D) of the ellipsoidal, transversal sections (obtained from entire field views, such as those shown in Figs. 1, 2, 5a). The average dimensions of barreloids and whiskers in young and adult rats are depicted in Figures 7–9.

In young rats, whisker length decreased along the rows (from arc 0 to arc 4) and increased along the arcs from rows A–C (Fig. 7). In rows C–E, the whisker lengths were

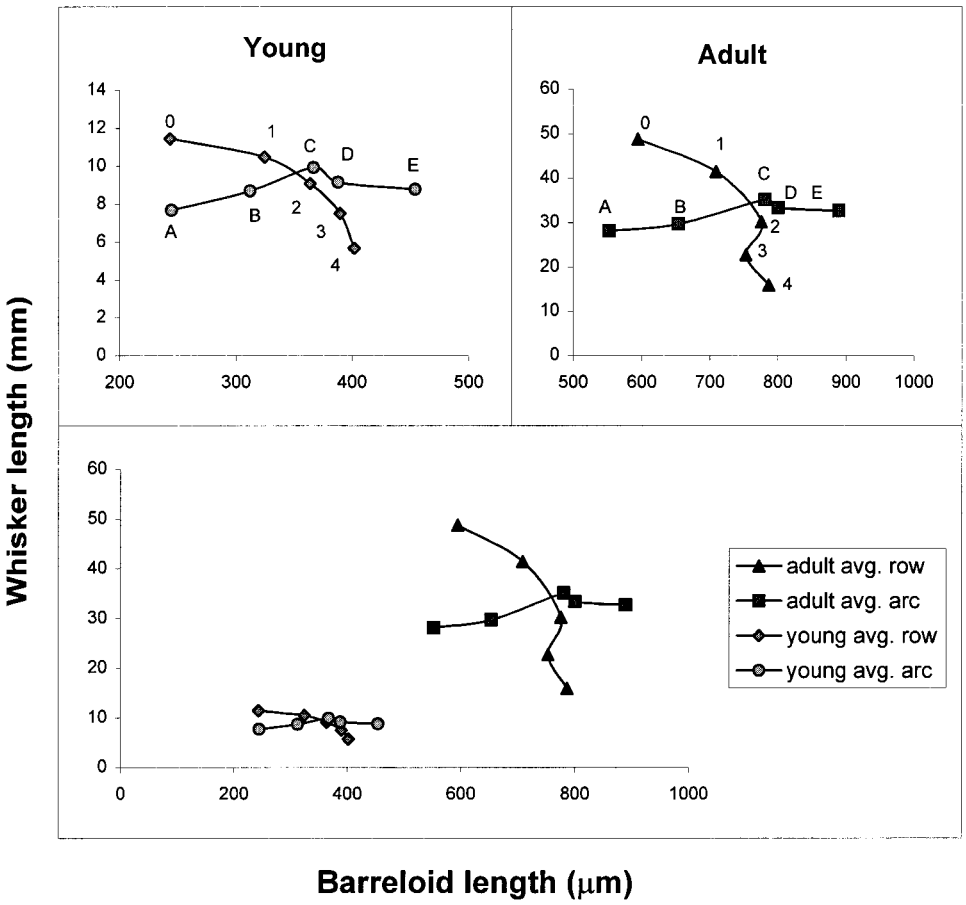

Fig. 10. Relationships of the average lengths of barreloids and whiskers along rows and arcs in young and adult rats. Mean values across all rows and arcs are shown using the same data that were used for Figures 7 and 8.

similar. The diameters of the whisker follicles decreased along the rows and increased along the arcs. However, the pattern of the length of the barreloids in the young rats was different than that of their whiskers. In rows C–E and arcs 2–4, the lengths of their barreloids increased continuously from arc 0 to arc 4 and from row A to row E, respectively, whereas, in the other rows and arcs, it plateaued.

The patterns of barreloid and whisker dimensions in adult rats (Fig. 8) were similar to those observed with young rats, except that, in adults, 1) arc 1 seemed to behave like arcs 2–4; 2) the dimensions of barreloid lengths in the rows C–E and arcs 2–4 were more uniform; 3) whisker length along each arc was more uniform; and 4) the follicle sizes of straddlers were similar to those of arc 1. In both young rats and adult rats, the diameters (d and D) of the barreloids in the field view were essentially uniform (Fig. 9), indicating that the volume of the barreloids is related directly to their length (Figs. 7, 8).

Along rows and arcs, an opposite relation was observed between the mean length of barreloids and mean whisker sizes (Figs. 10, 11). The largest barreloids did not represent the largest whiskers. Rather, the largest barreloids represented the nine whiskers C2–C4, D2–D4, and E2–E4 in both young rats and adult rats.

DISCUSSION

Vibrissal representation in the VPM

This is the first report of visualization, in consecutive thalamic slices, of the entire tactile vibrissal representation in the VPM. This was achieved by defining three cutting planes through the VPM that were perpendicular to each other: oblique horizontal (Fig. 5g) for the visualization of the entire barreloid field, oblique sagittal (Fig. 5h) for the visualization of individual arcs, and oblique coronal (Fig. 5i) for the visualization of individual rows.

In adult mice, Zantua et al. (1996) observed a lack of demarcation of the barreloid pattern, an increase in the size of the VPM, tripling of the segment length of dendritic branches, and doubling of the number of dendritic segments compared with young mice. In our histological preparations of the rat brain, the observed organization of the VPM suggested that either the same process or a similar process occurs in rats upon aging. In fact, our visualization of barreloids in adult rats was not as distinct as that for barreloids in young rats. Nevertheless, the arrangement of barreloids in adult rats could be revealed using the optimal cutting angles we defined for the brains of young rats (Figs. 5, 6). When the absolute values of the length and of the two diameters of barreloids were com-

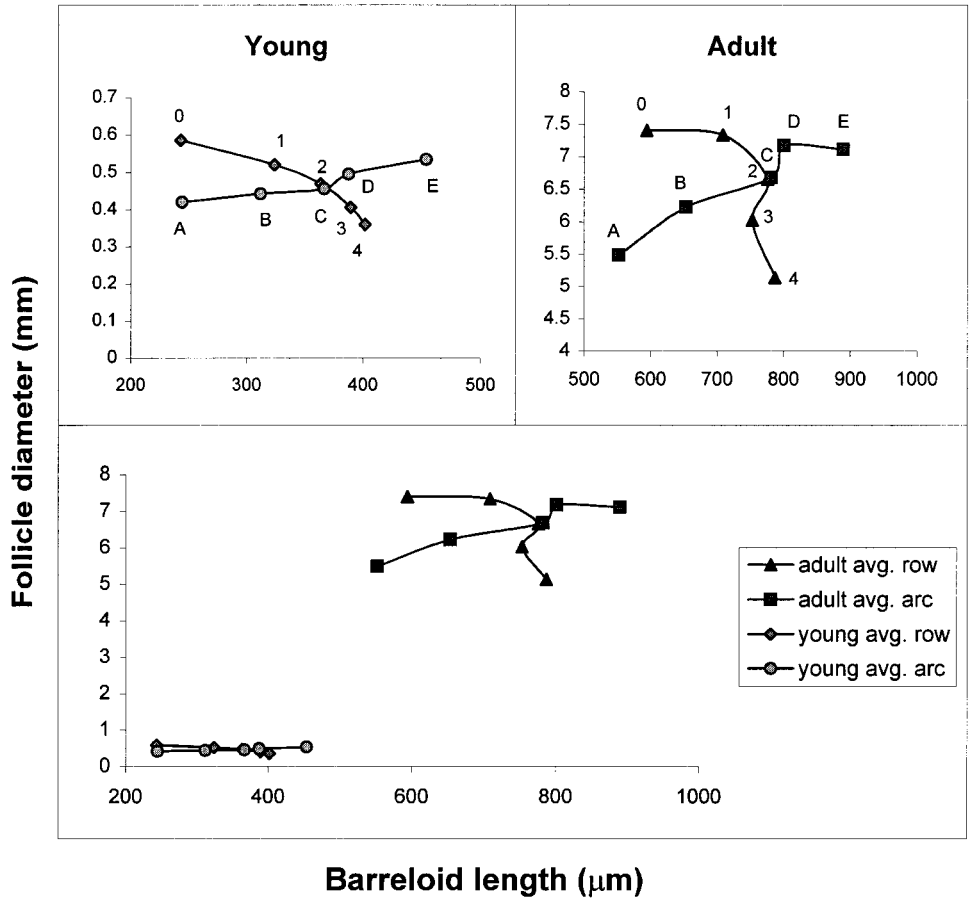

Fig. 11. Relationships of the average barreloid length and follicle diameter along rows and arcs in young and adult rats (for conventions, see Fig. 10, legend).

pared, each of them appeared to be approximately two times larger in adult rats than in young rats (Figs. 7–9).

In consecutive thalamic slices that were obtained using the oblique sagittal cutting plane (Fig. 5h), the entire array of arcs in the VPM (each arc occupied a complete section through the VPM) could be visualized (Fig. 3). The three-dimensional structure of the entire VPM, when viewed such that the visualization of arcs is optimal (not shown), appears to be a truncated pyramid in which the horizontal dimensions of each underlying disc are greater than of the disc above it. Positioned at the top of the pyramid is a disc that contains barreloids that represent the straddlers. The disc under it is composed of barreloids that represent vibrissae of only the first four rows, because barreloid E1 was almost (but not quite) in line with barreloids A2, B2, C2, and D2 in the third arc. This phenomenon of the anterior parts of the arcs shifting in the ventromedial direction appeared in all of our sections with barreloid arcs (see Figs. 3, 6).

Similarly, the three-dimensional structure of the VPM, when viewed such that the visualization of rows is optimal [i.e., using consecutive slices obtained using the oblique coronal cutting plane (Fig. 5i); not shown], resembles a truncated pyramid: The first four barreloids in each row appear like regularly arranged, straight cylinders, the lengths of which increase from dorsolateral to ventromedial, with clearly seen septa. In the ventromedial part of these "pyramids," thin barreloids representing nasal vibrissae, thick barreloids that belong to rows D and E, and thin, long barreloids representing microvibrissae could be seen (see Fig. 4).

Schematic drawings of the barreloids usually assumed a uniform, rod-like shape of equal size for all barreloids (Sugitani et al., 1990, Land et al., 1995). The similarity of barreloid diameters in the coronal plane also was implied by the equal distances between the functional representations of the different whiskers along the row, as revealed by Waite (1973). This latter finding was challenged by Vahle-Hinz and Gottschaldt (1983), who concluded that the size of an individual thalamic representation field corresponds to the size of the respective sinus hair follicle. Our findings support an equidiameter size of barreloids (Fig. 9) but indicate that the lengths of barreloids vary significantly (Figs. 7, 8).

Comparison with previous results

The appearance of the barreloid field in adult rats was described first by Land and Simons (1985). Later, the detailed, three-dimensional structure of whisker representations was revealed using electrophysiological recordings (Sugitani et al., 1990). These results were confirmed by an anatomical study that also revealed the organiza-

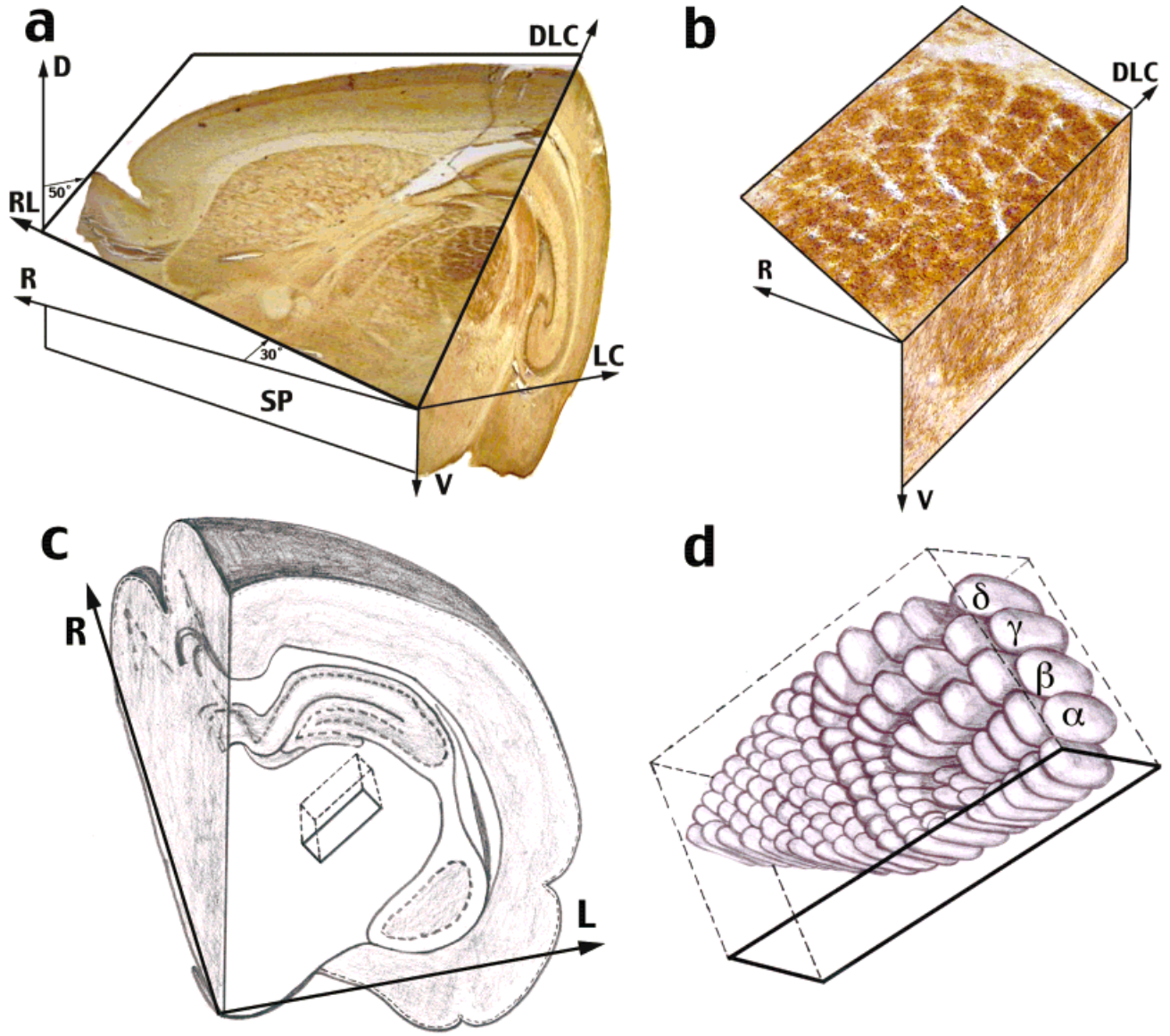

Fig. 12. Three-dimensional organization of the VPM of the rat. **a:** Photomontage demonstrating the three-dimensional arrangement of barreloids in the VPM of young (6-day-old) rats. The two CO-stained slices that are positioned perpendicular to each other were obtained from two individuals, and were cut according to the cutting planes depicted in Figure 5g,i. The entire barreloid field is revealed in the left slice, and a row of barreloids is contained in the other slice. The stereotaxic orientation is indicated by the arrows. **b:** Higher-magnification view of the region in "a" depicting individual barreloids in two planes. **c:** The orientation of the long axis of the VPM viewed from caudodorsal to ventrorostral in a schematic drawing of a coronal section through the right cerebral hemisphere of the rat cut at the caudal pole of the VPM (approximately −4.3 mm from Bregma). **d:** Three-dimensional reconstruction of the barreloids in the VPM based on the arrangement of barreloids in the entire field (see Fig. 1) and in individual arcs (see Figs. 3, 6). The location of this reconstruction within a coronal section is indicated by the box in c, with the plane (rectangle) marked by solid lines located at the caudal edge of the VPM. D, dorsal; DLC, dorsolaterocaudal; L, lateral; LC, laterocaudal; R, rostral; RL, rostrolateral; SP, sagittal plane; V, ventral; α, β, γ, and δ, straddlers.

tion of individual arcs in the VPM (Land et al., 1995). However, in none of these studies were the dimensions of barreloids quantitated. Furthermore, in no other previous study was the entire barreloid field in the VPM described using consecutive slices in all three major planes. The three-dimensional structure of the VPM revealed here is consistent with the general scheme revealed by Land and colleagues (Land and Simons, 1985; Land et al., 1995) and Sugitani et al. (1990) as well as with the earlier indications for such an arrangement (Van der Loos, 1976; Woolsey et al., 1979). However, our quantitative measurements and comprehensive visualization of all of the rows and the first five arcs revealed additional, important information about the structure and organization of barreloids. We found that barreloid lengths are not uniform, as suggested previously, but, rather, varied along the arcs and rows.

Size gradients of thalamic representations

The amount of vibrissal innervation decreases along the rows, from caudal to rostral (Lee and Woolsey, 1975; Welker and Van der Loos, 1986; Crissman et al., 1991). This decrease in innervation along the rows and the increased innervation along the arcs, from A–C (Welker and Van der Loos, 1986), indicates that the amount of innervation in general is correlated with whisker length and follicle diameter (Figs. 7, 8). These gradients of innervation across the mystacial pad correlate nicely with the size gradients of cortical barrels (Lee and Woolsey, 1975; Welker and Van der Loos, 1986; Rice, 1995). Thus, it was expected that size gradients in the VPM would exhibit a similar pattern.

Interestingly, the size gradients of barreloids that we found in the VPM did not follow the same pattern. Although the size gradients of barreloids along the arcs did correlate with those of the whiskers, the size gradients of barreloids and whiskers along the rows were reversed. Barreloid size increased along the row, whereas whisker length, follicle size (Figs. 7, 8), and axonal innervation decreased (Lee and Woolsey, 1975; Welker and Van der Loos, 1986; Crissman et al., 1991). Thus, the largest whiskers in the mystacial pad (the straddlers) had the smallest representations in each row of barreloids (Figs. 4, 6–8) in the DLBSF.

These inverse gradients produce a thalamic magnification pattern that is different from the patterns observed in the mystacial pad and barrel cortex. The largest representations in the VPM are those of the nine whiskers C2–C4, D2–D4, and E2–E4 (Fig. 10); whereas, in the periphery and cortex, the largest representations are those of the most caudal whiskers of rows C–E. The magnification of the representations of the more rostral whiskers probably begins at the brainstem (Shortland et al., 1996). This thalamic magnification pattern, the detection of which required the visualization of entire individual rows and arcs in the planes that expose the long barreloid axes, escaped previous careful mapping attempts using qualitative anatomical mapping (Land et al., 1995) and electrophysiological mapping techniques (Waite, 1973; Vahle-Hinz and Gottschaldt, 1983; Sugitani et al., 1990).

Three-dimensional organization of the VPM

The angles used to cut brain sections are crucial for visualizing barreloids, as was first shown by Van der Loos (1976). However, even with the optimal cutting planes that Van der Loos defined (0–10° anteriorly and 15–25° laterally) for sectioning mouse brains, a tilting of the slide on the microscope stage at an angle of up to 45° further improved visualization of barreloids. In the rat, a rotation of the thalamus by approximately 45° from the horizontal plane provides a view of the barreloids field (Land et al., 1995). However, in our hands, it appeared that a rotation around one axis was not sufficient for the visualization of the entire barreloid field. In our experiments, when the arcs of the barreloids were visualized (Figs. 3, 6) by cutting at an angle of 40° counterclockwise to the sagittal plane, the medialmost ends of the barreloids formed an angle of about 30° to the sagittal plane (Fig. 5e). When this angle was considered and was used for cutting horizontal oblique slices in addition to lateral tilting of 50° (Fig. 5g), the entire barreloid field was obtained in both young animals (Fig. 1) and adult animals (Fig. 5a). Cutting vertically at an angle of 30° to the coronal plane consistently resulted in the visualization of entire rows of barreloids in serial slices.

The stereotaxic orientation of the barreloid field and of the long axes of individual barreloids can be visualized using composite photomontages of slices from brains of young rats (Fig. 12a,b). When viewed dorsocaudally (Fig. 12c), the barreloids stained for CO form a cluster that is reminiscent of a pine cone with its tip oriented ventromedially (Fig. 12d).

CONCLUSIONS

The barreloid field in the VPM appeared to consist of two parts: the DLBSF, which contains thick barreloids that represent mystacial vibrissae, and the ventromedial part, which contains thin barreloids that represent nonmystacial sinus hairs. In both young rats and adult rats, the VPM appeared to have a similar barreloid arrangement; however, visualization of the entire VPM as well as individual barreloids was clearer in the young animals. In adult rats, the lengths (L) and diameters (d and D) of individual barreloids were each about twice the values of those observed in young rats, and the barreloid cores appeared heteromorphous because of increased sizes of endogenous and exogenous bundles of myelinated nerve fibers. In both young rats and adult rats, the representations of whiskers in the middle of rows C–E, which were not the most innervated, were maximal.

ACKNOWLEDGMENTS

S.H. was supported by the Center for Absorption of Scientists, Ministry of Absorption, Israel. We thank E. Gamzu for assisting with data analysis, R. Malach for helpful comments, and B. Schick for reviewing this article.

LITERATURE CITED

Ahissar E, Zacksenhouse M. 2000. Temporal and spatial coding in the rat vibrissal system. Progr Brain Res (in press).

Ahissar E, Sosnik R, Haidarliu S. 2000. Transformation from temporal to rate coding in a somatosensory thalamocortical pathway. Nature 406: 302–6.

Belford GR, Killackey HP. 1979. Vibrissae representation in subcortical trigeminal centers of the neonatal rat. J Comp Neurol 183:305–322.

Brecht M, Preilowski B, Merzenich MM. 1997. Functional architecture of the mystacial vibrissae. Behav Brain Res 84:81–97.

Chmielowska J, Carvell GE, Simons DJ. 1989. Spatial organization of thalamocortical and corticothalamic projection systems in the rat SmI barrel cortex. J Comp Neurol 285:325–338.

Crissman RS, Warden RJ, Siciliano DA, Klein BG, Renehan WE, Jacquin MF, Rhoades RW. 1991. Numbers of axons innervating mystacial vibrissa follicles in newborn and adult rats. Somatosen Motor Res 8:103–109.

Haidarliu S, Ahissar E. 1997. Spatial organization of facial vibrissae and cortical barrels in the guinea pig and golden hamster. J Comp Neurol 385:515–527.

Haidarliu S, Sosnik R, Ahissar E. 1999. Simultaneous multi-site recordings and iontophoretic drug and dye applications along the trigeminal system of anesthetized rats. J Neurosci Methods 94:27–40.

Ivy GO, Killackey HP. 1982. Ephemeral cellular segmentation in the thalamus of the neonatal rat. Brain Res Dev Brain Res 2:1–17.

Land PW, Simons DJ. 1985. Metabolic and structural correlates of the vibrissae representation in the thalamus of the adult rat. Neurosci Lett 60:319–324.

Land PW, Buffer SA, Yaskosky JD. 1995. Barreloids in adult rat thalamus:

three-dimensional architecture and relationship to somatosensory cortical barrels. J Comp Neurol 355:573–588.

Lee K, Woolsey TA. 1975. A proportional relationship between peripheral innervation density and cortical neuron number in the somatosensory system of the mouse. Brain Res 99:349–353.

Lu SM, Lin RC. 1993. Thalamic afferents of the rat barrel cortex: a light- and electron-microscopic study using *Phaseolus vulgaris* leucoagglutinin as an anterograde tracer. Somatosens Motor Res 10:1–16.

Ma PM. 1991. The barrelettes—architectonic vibrissal representations in the brainstem trigeminal complex of the mouse; a normal structural organization. J Comp Neurol 309:161–199.

Price JL. 1995. Thalamus. In: Paxinos G, editor. The rat nervous system. San Diego: Academic Press. p 629–648.

Rice FL. 1995. Comparative aspects of barrel structure and development. In: Jones EG, Diamond IT, editors. Cerebral cortex, vol 11. New York: Plenum Press. p 1–75.

Shortland PJ, Demaro JA, Shang F, Wait PME, Jacquin MF. 1996. Peripheral and central predictors of whisker afferent morphology in the rat brainstem. J Comp Neurol 375:481–501.

Sugitani M, Yano J, Sugai T, Ooyama H. 1990. Somatotopic organization and columnar structure of vibrissae representation in the rat ventrobasal complex. Exp Brain Res 81:346–352.

Vahle-Hinz C, Gottschaldt K-M. 1983. Principal differences in the organization of the thalamic face representation in rodents and felines. In: Macchi G, Rustioni A, Spreafico R, editors. Somatosensory integration in the thalamus. Amsterdam: Elsevier. p 125–145.

Van der Loos H. 1976. Barreloids in mouse somatosensory thalamus. Neurosci Lett 2:1–6.

Waite PME. 1973. Somatotopic organization of vibrissal responses in the ventro-basal complex of the rat thalamus. J Physiol 228:527–540.

Welker E, Van der Loos H. 1986. Quantitative correlation between barrelfield size and the sensory innervation of the whiskerpad: a comparative study in six strains of mice bred for different patterns of mystacial vibrissae. J Neurosci 6:3355–3373.

Wong-Riley M. 1989. Cytochrome oxidase: an endogenous metabolic marker for neuronal activity. Trends Neurosci 12:94–101.

Woolsey TA, Van der Loos H. 1970. The structural organization of layer IV in the somatosensory region (SI) of mouse cerebral cortex: the description of a cortical field composed of discrete cytoarchitectonic units. Brain Res 17:205–242.

Woolsey TA, Anderson JR, Wann JR, Stanfield BB. 1979. Effects of early vibrissae damage on neurons in the ventrobasal (VB) thalamus of the mouse. J Comp Neurol 184:363–380.

Yamakado M. 1999. Reassemblage of primary cell aggregates and modulation of subcortical connections in the thalamic relay nucleus: effects of vibrissal damage in the developing whisker-to-barrel pathway in the mouse. J Comp Neurol 403:517–533.

Zantua JB, Wasserstrom SP, Arends JJA, Jacquin MF, Woolsey TA. 1996. Postnatal development of mouse "whisker" thalamus: ventroposterior medial nucleus (VPM), barreloids, and their thalamocortical relay neurons. Somatosens Motor Res 13:307–322.